ACS APPLIED NANO MATERIALS

www.acsanm.org Article

Color Tuning of Electrochromic TiO_2 Nanofibrous Layers Loaded with Metal and Metal Oxide Nanoparticles for Smart Colored Windows

Cavit Eyovge,* Cristian S. Deenen, Francisco Ruiz-Zepeda, Stephan Bartling, Yury Smirnov, Monica Morales-Masis, Arturo Susarrey-Arce,* and Han Gardeniers*

Cite This: *ACS Appl. Nano Mater.* 2021, 4, 8600–8610 Read Online

ACCESS | Metrics & More | Article Recommendations | Supporting Information

ABSTRACT: Co-axial electrospinning was applied for the structuring of non-woven webs of TiO_2 nanofibers loaded with Ag, Au, and CuO nanoparticles. The composite layers were tested in an electrochromic half-cell assembly. A clear correlation between the nanoparticle composition and electrochromic effect in the nanofibrous composite is observed: TiO_2 loaded with Ag reveals a black-brown color, Au shows a dark-blue color, and CuO shows a dark-green color. For electrochromic applications, the Au/TiO_2 layer is the most promising choice, with a color modulation time of 6 s, transmittance modulation of 40%, coloration efficiency of 20 cm^2/C, areal capacitance of 300 F/cm^2, and cyclic stability of over 1000 cycles in an 18 h period. In this study, an unexplored path for the rational design of TiO_2-based electrochromic device is offered with unique color-switching and optical efficiency gained by the fibrous layer. It is also foreseen that co-axial electrospinning can be an alternative nanofabrication technique for smart colored windows.

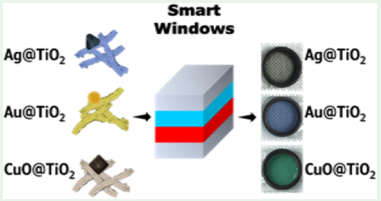

KEYWORDS: *electrochromism, electrospinning, co-axial fibers, nanoparticles, color tuning*

1. INTRODUCTION

Electrochromic (EC) color modulation is a widely applied technology in the energy-efficient sector with a high energy-saving potential. The technology is currently implemented in smart buildings, airplane windows, self-dimming rear mirrors, and energy storage devices.[1] Typically, the assembly of an EC device (ECD) is a composition of different layered materials where light transmission properties are altered upon the application of an electrical potential difference.[1] An ECD consists of three conductive elements: an EC layer, an ionically conductive electrolyte, and an ion storage layer, which are sandwiched between two optically transparent and conductive substrates. In this configuration, coloration/bleaching takes place in the EC layer, for which composition varies upon functionality, ranging from metal coordination complexes to conjugated conducting polymers and to transition metal oxides.[2,3] Among them, transition metal oxides like WO_3 and TiO_2 are low-cost and promising options for which chemistry can be tuned by wet coating deposition or by other means applied to thin film technology (e.g., plasma deposition,[4] magnetron sputtering,[5] and electron beam evaporation[6]). Despite its moderate stability and complex stoichiometry, WO_3 is the common material for EC layers. On the contrary, TiO_2 is less frequently used owing to its poor coloration performance.[7] The research ongoing for higher performance TiO_2-based electrochromic devices proved that it is possible to improve electrochromic response of the TiO_2 by modifying the TiO_2 electrode structures.[8,9]

Common strategies to improve optical properties in the EC layer are nanostructuring,[10,11] composite formation,[12] and metal oxide doping.[13,14] It is also possible to unlock properties that are not attainable by the WO_3 or TiO_2 materials on their own by employing one, or a combination of these methods. For example, composite (photo)EC layers have attracted enormous attention owing to their intriguing physical properties, particularly with the fabrication of WO_3 films of varied compositions (Pt,[15] Ti,[16,17] Au,[18,19] or Ag[20,21]). It has been observed that the addition of metal NPs to the semiconductor can either diminish or increase EC coloration performance. Enhancements in (photo)EC properties such as short coloration/bleaching time and increased coloration efficiency are highly related to the increased surface conductivity by electronic confinement of the (photo)EC layer material, and, in some cases, also assisted by the surface plasmonic resonance phenomenon for coloration improvement. Additionally, it is also proved that when metal NPs having different Fermi energy levels are in contact with TiO_2, the band structure of the NP/TiO_2 changes such that an S-shaped potential curve is formed due to the difference in chemical potentials. For the case of Au

Received: July 30, 2021
Accepted: August 6, 2021
Published: August 16, 2021

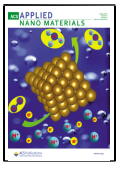

Scheme 1. Fabrication Protocol for the NP-Composited TiO_2 fibers Showing (1) Co-Axial Electrospinning, (2) Heat Treatment in Air, and (3) EC Device Integration and Functionality

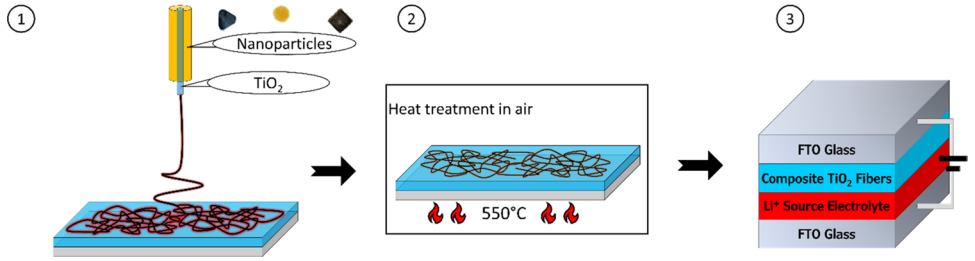

NPs, an upward band bending is observed, which in turn accumulates holes at the TiO_2 surface, while for Ag NPs, a downward bending is presented, leading to the accumulation of electrons. Semiconducting metal oxide NPs on the other hand, will result in heterojunction formation when coupled with TiO_2, and similar to the metal NPs, will alter the band structure of the composite unit. Schematic representations of band bending with Ag and Au NPs are also provided in Scheme S1. One of the widely studied heterojunctions of this case is CuO/TiO_2, in which more efficient charge separation is observed together with a lower band gap energy in the composite form. Even though it is mostly studied for photocatalysis,[22] possible bending outcomes have not been explored thoroughly for the TiO_2 structures.

Although it is quite advantageous to modify the chemical composition of the EC layers, there is a limited number of methods that allow one-step sculpting of nanofiber-like structures of varied material combinations. Besides the well-known one-pot synthetic approaches, an excellent candidate is co-axial electrospinning. Its application in EC layers is atypical; until now, the technique has been mostly applied in the biomedical field.[23] Additionally, applications of electrospinning in the energy storage and conversion areas have already been promoted.[24,25] In the past, fibrous or 1D morphologies have been shown to be of use for electrochemical redox reactions, where charge transfer occurs much faster compared to thin film technology.[26,27] Furthermore, layering composite fibrous layers can also be beneficial to enhance light transmission and light modulation.[28,29]

Here, the advantages of electrospinning in EC switchable glass with the formulation of metal NP-loaded TiO_2 composite nanofibers are showcased. The TiO_2 nanofibers were decorated with Ag, Au, and CuO NPs to enhance optical absorption properties and accelerate color-switching and modulation in ECDs. Effects of modified band structures with Ag (downward band bending), Au (upward band bending), and CuO (heterojunction band bending) on electrochromic color change are also evaluated by forming three different NP/TiO_2 composite structures. Transmission electron microscopy (TEM) and scanning electron microscopy (SEM) were used to depict the morphology of the composite nanofibers. Ultraviolet−visible−near infrared spectroscopy (UV−vis−NIR) was employed to generate knowledge on the optical characteristics of the TiO_2 nanofibrous layers loaded with metal and metal oxide NPs. Electrochemical and electrochromic properties were investigated in-depth to allow us to estimate ECD coloration time, transmittance modulation, areal capacitance, and cyclic stability. Our results reveal that color tuning in NP/TiO_2 nanofibers is possible, such that Ag shows a black-brown color, Au yields dark-blue, and CuO leads to a dark-green color under negative bias. Among the different TiO_2 layers loaded with NPs, the Au/TiO_2 composite yields the most prominent electrochemical activity with an anodic current density of 1.81 mA/cm^2 and the areal capacitance of 300 F/cm^2 with the most efficient optical density change of 40%. Moreover, the electrochromic lifetime of the Au-composited EC layers is found to be at least 1000 cycles measured within an 18 h period, with the fastest modulation time of 6.1 and 8.1 s for coloration and bleaching, respectively. The results obtained are found to pair-up with coloration/bleaching times reported in the literature. The rational design of TiO_2 layers loaded with NPs for coloration modulation, attainable with co-axial electrospinning, offers an unexplored path for the design of EC layers and devices. Our results in combination with the reported scalability of electrospinning demonstrate the potential of larger scale EC layers for smart colored windows.

2. EXPERIMENTAL SECTION

2.1. Co-Axial Electrospinning of TiO_2 Nanofibers Loaded with Metal/Metal Oxide Nanoparticles. Co-axial electrospinning was used for the synthesis of the NP-loaded composite TiO_2 nanofibers. In short, the methodology involves two syringes feeding liquid interseparately, i.e., inner fluid and outer fluid (co-axially) to a spinneret.[30] Under the application of a potential difference between the spinneret and the collector, the liquid is drawn out co-axially from the spinneret forming a Taylor cone composed of a core (from the inner fluid) and a shell (outer fluid). In this way, a core−shell liquid thread is formed, which, due to the evaporation of the solvent, ends at the collector electrode in a dried form (Scheme 1, step 1). A solution of 7% (w/v) PVP in ethanol was used as the core formulation, which was prepared by first dissolving 700 mg of PVP (CAS no, 9003-39-8, 1,300,000. Mw, Sigma Aldrich) in 10 mL of absolute ethanol (CAS no. 64-17-5, 99.8%, Sigma Aldrich). The suspension was left under magnetic stirring for 3 h at room temperature. After 3 h, TiO_2 nanopowder (CAS no. 13463-67-7, 99.5%, Sigma Aldrich) was added to the solution reaching 10 mg/mL concentration. Continuous ultrasonication was applied for 3 h for obtaining a white suspension.

Next, the shell NP precursor solutions were prepared following a similar route but by mixing 7% (w/v) PVP/ethanol with either (i) Ag (0.02 mg/mL in suspension, CAS no. 7440-22-4, nanoComposix), (ii) Au (0.05 mg/mL in suspension, CAS no. 7440-57-5, Sigma Aldrich), or (iii) CuO (0.1 mg/mL in suspension, CAS no. 1317-38-0, nanoComposix). NPs and PVP are mixed to have a final concentration of 0.05 mg/mL for the NPs in the final precursor. Note that for the Ag-containing precursor, centrifugation was used to increase the Ag content up to the desired value. Samples were sonicated for 3 h to obtain green, pink, or yellow precursor, respectively. Thanks to the low concentration of metal/metal oxide NPs at the shell precursor, deviations related to electrospinning parameters were minimized.

Electrospinning was carried out using a co-axial nozzle (IME Technologies, the Netherlands) in a home-made setup. The nozzle was kept at 18 kV during electrospinning, and resulting fibers were

https://doi.org/10.1021/acsanm.1c02231
ACS Appl. Nano Mater. 2021, 4, 8600−8610

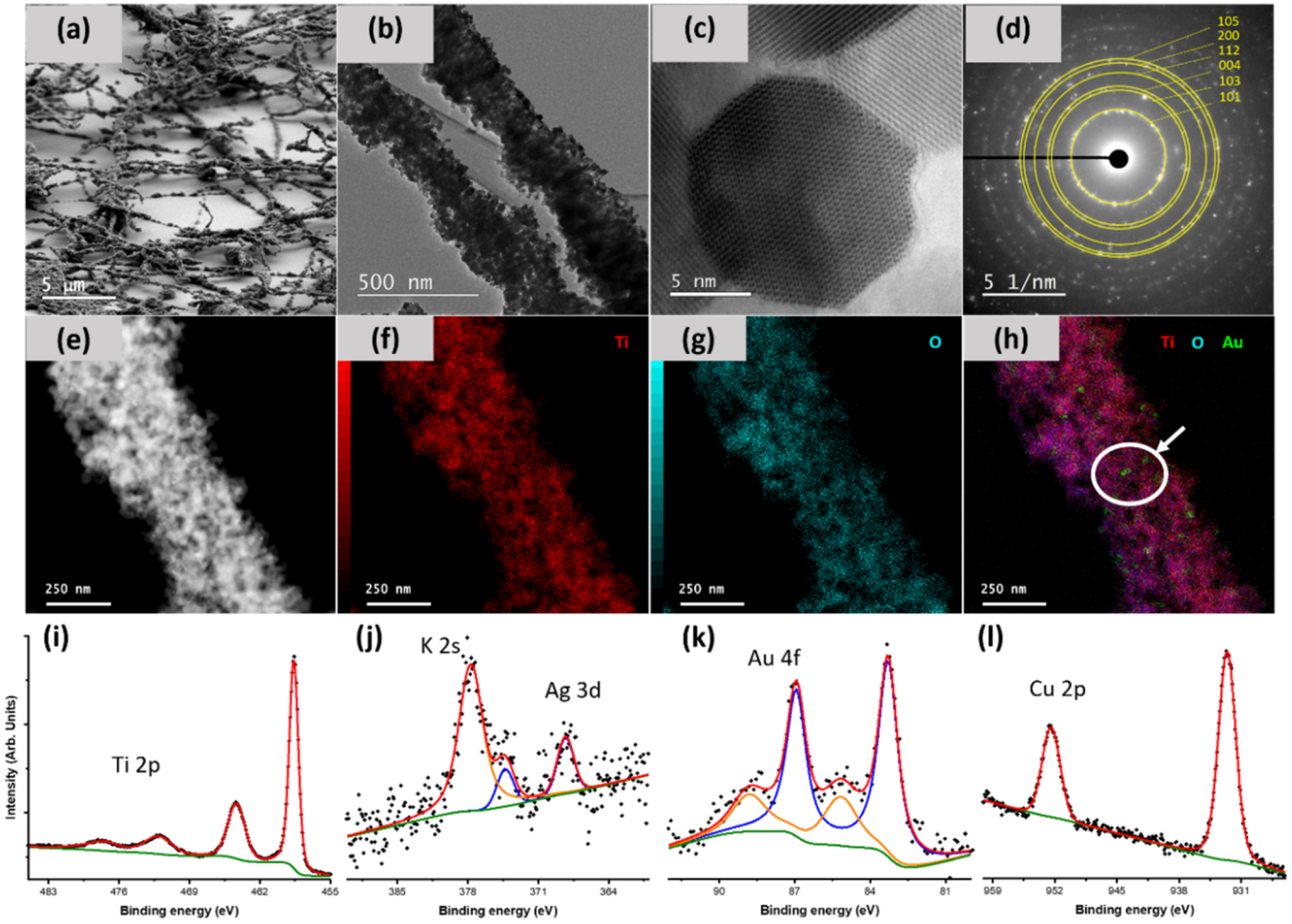

Figure 1. (a) SEM and (b) TEM images of the TiO_2 nanofibers. (c) SAED pattern of TiO_2 nanofibers with indicated anatase planes. (d) Close-up STEM BF image of a single grain and a grain boundary (marked) between the crystallites composing the TiO_2 nanofibers. (e) STEM ADF image of one Au/TiO_2 composite nanofiber. The corresponding STEM-EDX maps are (f) Ti signal in red, (g) O signal in cyan, and (h) Au signal in green overlaid with Ti and O signals. The presence of the Au nanoparticles in the TiO_2 nanofiber is highlighted. High-resolution XPS spectra of (i) TiO_2 nanofibers loaded with (j) Ag, (k) Au, and (l) CuO nanoparticles. The TiO_2 nanofibers with and without NPs are measured after thermal annealing. The collected data is processed (as shown in red lines) considering the baseline, which are given as green lines in the spectra together with located peaks.

collected on top of fluorine-doped tin oxide (FTO)-coated glass substrates, which were kept at −1 kV. The working distance between the co-axial nozzle and the substrates was kept constant at 12 cm, and an electrospinning duration of 2 min was employed for all the samples. The thicknesses of the electrospun layers were estimated at ca. 1 μm.

The nanofibers were heat treated to remove the PVP in a two-step procedure in air. The main reason for annealing here is to remove the non-conductive polymeric content. PVP is only used as a binder for TiO_2 NPs to form fibers, and its existence in the final devices will prohibit Li^+ intake/release during coloration/bleaching. Therefore, PVP within the fibers should be removed with a heat treatment process to have only electrochromically active materials. In the first step of the heat treatment, samples were heated up to 350 °C with 1 °C/min heating rate and kept for 3 h at that temperature. The second step was heated up to 550 °C with the same heating rate and kept for 1 h. Afterward, controlled cooling with 1 °C/min was applied to obtain the final EC layers (Scheme 1, step 2). Next, EC layers were integrated into an electrochemical cell to test device functionality (Scheme 1, step 3). For detailed information about device integration and functionality, please see section 2.5.

2.2. Morphological Characterization. The morphologies of the composite samples were characterized by SEM (Carl Zeiss, Merlin AURIGA CrossBeam Workstation). Top-view and cross-sectional-view images were recorded using an in-lens detector and an acceleration voltage of 1.4 kV. Scanning transmission electron microscopy (STEM) and energy dispersive X-ray spectrometry (EDX) were carried out using a Cs-corrected microscope CF-ARM Jeol 200 equipped with an SSD Jeol EDX spectrometer. The operational voltage employed was 200 kV. A special set of TiO_2 fibers were electrospun over Au grids and thermally annealed, as described above for this characterization. The grid was inspected under TEM before and after annealing.

2.3. Structural Characterization. X-ray diffraction (XRD) analysis was carried out with a diffractometer (Bruker D8 Advance) operated at 30 kV, 10 mA at 2θ (Cu Kα, (λ = 0.15418 nm) 20−65°, employing a step size of 0.02° with a scan speed of 2.5°/min.

2.3.1. Surface and Chemical Analysis. The X-ray photoelectron spectroscopy (XPS) measurements were performed (ESCALAB 220iXL, Thermo Fisher Scientific) with monochromated Al Kα radiation (E = 1486.6 eV). The nanofibers deposited on silicon wafers are prepared on a stainless-steel holder with conductive double-sided adhesive carbon tape. The electron binding energies were obtained with charge compensation using a flood electron source and referenced to the C 1s core level of adventitious carbon at 284.8 eV (C−C and C−H bonds). For quantitative analysis, the peaks were deconvoluted with Gaussian−Lorentzian curves using the software Unifit 2020. The peak areas were normalized by the transmission

https://doi.org/10.1021/acsanm.1c02231
ACS Appl. Nano Mater. 2021, 4, 8600−8610

function of the spectrometer and the element-specific sensitivity factor of Scofield.[31] The valence band spectra of bare and NP-incorporated TiO_2 fibers were evaluated after recording ultraviolet photoelectron spectroscopy (UPS). The He I (21.22 eV) excitation line and a negative bias of 10 V were used to separate secondary electrons originating from the sample and spectrometer and to estimate the absolute work function value from the high BE cut-off region of the UPS spectra.

2.4. Optical Characterization. The optical characterization was performed with a UV−vis−NIR spectrophotometer (PerkinElmer Lambda 950 UV−vis−NIR) in the 250 to 900 nm range, employing an integrating sphere. UV−vis spectra were recorded before and after the coloration. The transmittance (T) and the reflectance (R) spectrum were collected separately to estimate the absorptance spectrum of the fibrous layers. The absorptance (A) spectra were calculated using eq 1. To this end, the band gap was calculated with the Tauc method,[32] which involves plotting the $(\alpha h\nu)^{1/n}$ versus $(h\nu)$. The Tauc plot is derived from eq 2,[33] where α is the absorption coefficient, $h\nu$ is the photon energy, E_g is the band gap, and B is the proportional constant. The value of the exponent n denotes the nature of the optical transition (i.e., indirect or direct band gap); the value of which for this study is 2, considering indirect allowed transition.[32] A linear region was used to extrapolate to the x-axis intercept to find the band gap values. In a typical experiment, the T and R spectrum of the TiO_2 fibers with(out) NPs (Ag, Au, and CuO) were recorded. Similarly, the T and R for the FTO-coated glass used as reference were recorded (Figure S1). The data were treated following eq 1 for A, and then eq 2 for E_g.

$$A = 100 - (T + R) \tag{1}$$

$$(\alpha h\nu)^{1/n} = B(h\nu - E_g) \tag{2}$$

2.5. Electrochemical Characterization. Cyclic voltammetry (CV) and chronoamperometry (CA) were carried out in a three-electrode system containing 0.5 M lithium perchlorate ($LiClO_4$) (CAS no. 7791-03-9, 98.0%, Sigma Aldrich) in propylene carbonate (PC) (CAS no. 108-32-7, 99.7%, Sigma Aldrich) as the electrolyte. A Pt mesh of 4 cm^2 (CAS no. 7440-06-4, 99.9%, Alfa Aesar) was used as a counter electrode with a Ag/AgCl reference electrode. The working electrode was the EC layer containing either TiO_2- or NP-containing TiO_2 nanofibers over FTO (Scheme 1, step 3). CV and CA were recorded using a handheld potentiostat/galvanostat (PalmSens V2 Electrochemical Interface). The CV scans were carried out in the potential range of ±2 V with a scanning rate of 50 mV/s at room temperature. For color modulation tests, the CA was carried out by cycling between ±2 V with 30 s between coloration and bleaching. Electrochemical impedance spectroscopy (EIS) mas also measured with the same setup by an AC voltage of 5 mV amplitude at a frequency range of 1 MHz−1 Hz.

The changes in absorption spectra were measured by mounting the ECD to the UV−vis spectrophotometer. The coloration efficiency (CE) is defined as the change in optical density (ΔOD) per measured unit of the intercalated ionic charge (ΔQ) into an EC layer. CE and ΔOD can be obtained from eqs 3 and 4, where T_b and T_c refer to the transmittances of the layer in its bleached and colored states at 700 nm, respectively. In addition to that, coloration and bleaching times (t_c and t_b) of the ECDs were measured as the amount of time required to reach the corresponding T_c and T_b values.

$$\mathrm{CE} = \frac{\Delta \mathrm{OD}}{\Delta Q} \tag{3}$$

$$\Delta \mathrm{OD} = \log\left(\frac{T_b}{T_c}\right) \tag{4}$$

3. RESULTS AND DISCUSSION

3.1. Metal/Metal Oxide-Loaded TiO_2 Nanofibers. The structural characterization of the EC layer is addressed first to gain knowledge on the structure and composition of the TiO_2 nanofibers and explore the relationship of the coloration mechanism exerted by the constituents. Side-view SEM images of the EC TiO_2 layer are presented in Figure 1a. The TiO_2 layer is composed of randomly distributed TiO_2 nanofibers of ca. 200 ± 20 nm diameter. The nanofibers are stacked, forming a three-dimensional (3D) nanofiber mat architecture with the first nanofiber layer in contact with the FTO substrate (Figure S2). The morphology of such an open 3D structure is ideal for easy access to chemicals, like the EC electrolytes.

Table 1. Relative Ratio of % at. of the Compositing NPs to the Ti Measured via XPS

NP type/Ti	% at. ratio
Ag/Ti	0.007
Au/Ti	0.005
Cu/Ti	0.025

A detailed inspection with SEM and TEM imaging in Figure 1a,b indicates that the nanofibers are composed of nano agglomerates with a particle mean size of 25 nm (Figure S3). A closer look into the fiber in Figure 1d displays a TiO_2 crystallite with the anatase phase (Figure S4) and the boundaries with surrounding grains of different orientations, evidencing the high degree of polycrystallinity. This is confirmed by the ring pattern in the selected area electron diffraction (SAED) in Figure 1c, where yellow circles are used to highlight the (101), (103), (004), (112), (200), and (105) crystallographic lattice planes to identify the anatase phase of TiO_2. However, the presence of the rutile phase was also measured within the fibers, as shown in Figure S4. The results are in accordance with the XRD data in Figure S5.

The analysis of the chemical components and their spatial distribution in the metal-loaded nanofibers is assessed with STEM-EDX and XPS in Figure 1e−h and Figure 1i−l. Among the different metal loadings, nanofibers containing Au NPs are selected for STEM-EDX mapping. As shown in Figure 1f−h and Figure S6, the Au NPs are distributed along the TiO_2 nanofiber, in between the TiO_2 crystallites and on the surface. Most of them are located in a cluster-like manner (Figure S3b). Prior to the synthesis of the TiO_2 nanofibers, the NP diameter was 20 ± 4 nm (Figure S7), changing to average 4 ± 2 nm (Figure S3b) upon annealing in air. This can be rationalized as NP splitting into small pieces[34] owing to the imposed stress caused by the 3D fiber shrinkage during annealing[35] and would explain the fragmentation observed as the cluster-like feature of the Au NPs. Next, to understand the chemical characteristics of the Ag, Au, and CuO-loaded TiO_2 nanofibers, XPS analysis is performed (Figure 1i−l). The XPS spectrum for Ti 2p reveals two main peaks at 458.5 and 464.3 eV. The peaks are assigned to Ti(IV) from TiO_2.[36,37] For the metal NP-containing nanofiber, the Ag 3d, Au 4f, and Cu 2p spectrum was analyzed. The Ag 3d peaks at 368.3 and 374.3 eV are typically assigned to Ag.[38] However, Ag oxidation might occur due to heat treatment in air at 550 °C.[39] In this case, the typical binding energy of 367.7 eV for Ag_2O would be shifted by 0.6 eV, which would be in accordance with electron transfer from the Ag NPs to TiO_2 as expected for an Ohmic contact.[40] The peak at 377.7 eV is originated in K 2s, which probably left from the NP preparation process. The Au 4f region was fitted with two doublets, showing peaks at 83.3 and 86 eV (indicated with a red-colored line in Figure 1k), characteristic for metallic Au[41] as well as at 85.2 eV and 88.8 eV indicating oxidized Au

https://doi.org/10.1021/acsanm.1c02231
ACS Appl. Nano Mater. 2021, 4, 8600−8610

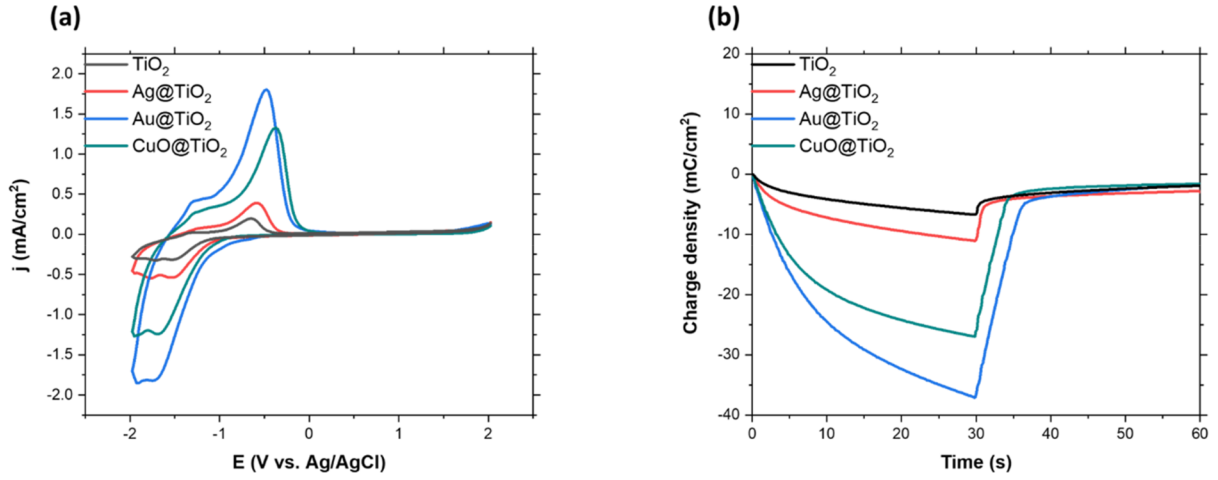

Figure 2. Comparative CV scans (a) and charge density change over time (b) of the EC layers.

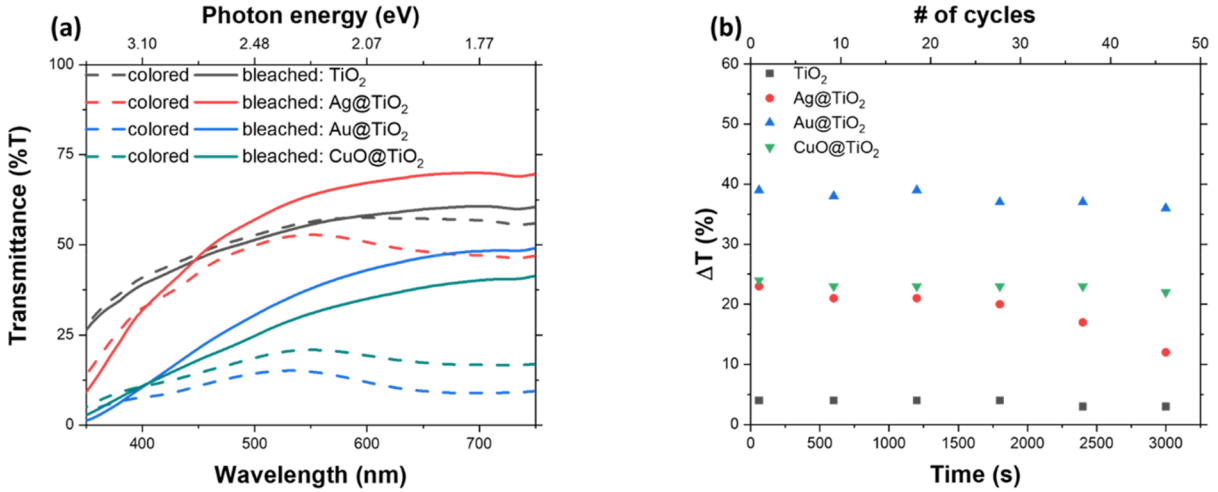

Figure 3. (a) Transmittance spectra recorded in the visible region for ECD devices in colored and bleached states within the first cycle. (b) Transmittance difference (ΔT) between colored (T_c) and bleached (T_b) states as a function of time (or the number of cycles). Note that absolute values of transmittance cannot be compared between different materials; instead, the change of transmittance in between colored an bleached states should be considered for device funcionality.

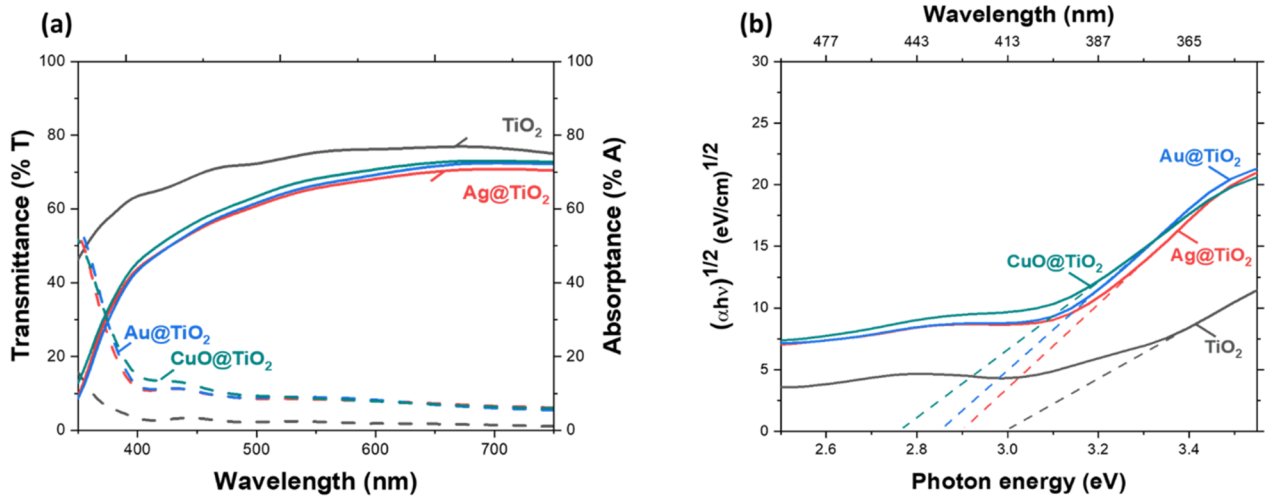

Figure 4. (a) Optical transmittance (left, *y*-axis) and absorptance (right, *y*-axis) as a function of wavelength measured for bare and metal (Ag, Au) and metal oxide NP (CuO) loaded TiO_2 nanofibers on the FTO substrate. The continuous lines are used for transmittance, while the dashed lines are used for absorptance. (b) Tauc plot derived from Ag/TiO_2, Au/TiO_2, and CuO/TiO_2 absorptance values. The Tauc plots are constructed to estimate the band gap of the different NP-loaded nanofibers.

https://doi.org/10.1021/acsanm.1c02231
ACS Appl. Nano Mater. 2021, 4, 8600−8610

Table 2. Electrochromic Properties of the ECDs Constructed[a]

	λ_{max} (nm)	ΔT (%)	t_c (s)	t_b (s)	ΔOD^a $\log(T_b/T_c)$	ΔQ^b (mC/cm^2)	CE^c (cm^2/C)
TiO_2	700	5	9.6	10.8	15.34	6.64	2.31
Ag/TiO_2	700	12	9.1	10.4	109.02	10.99	9.92
Au/TiO_2	700	40	6.1	8.1	890.09	37.01	24.05
CuO/TiO_2	700	23	8.7	9.6	377.87	26.15	14.45

[a](a) Optical density, (b) charge density, and (c) coloration efficiency values are calculated from the experimentally found data. Response times of coloration (t_c) and bleaching (t_b) are measured during the chronoamperometry cycles and provided here.

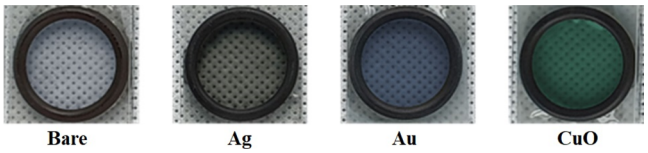

Figure 5. ECDs assembled by using an FTO-coated glass substrate as the counter. As it is depicted, the effect of different NPs on the attained color is clearly seen upon keeping the ECDs at −3 V. TiO_2 gives a pale blue color; Ag/TiO_2, Au/TiO_2, and CuO/TiO_2 yield brown, dark blue, and dark green colors, respectively.

(probably in the oxidation state 3^+).[42] Interestingly, when compared to the binding energy expected for Au $4f_{7/2}$ (84 eV),[43] a negative shift of ca. 0.7 eV is found. The negative shift can be related to electron transfer from oxygen vacancies of the TiO_2 to the Au NPs. For Cu 2p, the two main peaks at 932.6 and 952.4 eV without satellite peaks can be related to the presence of Cu_2O formed after annealing in air.[44]

The relative ratio of the NPs loaded into the electrospun TiO_2 fibers are also tabulated as % at. per probed area and given in Table 1 to verify the existence of compositing NPs within the annealed fibers. It is also important to mention that the inhomogeneous distribution of the NPs can vary the detected amounts in XPS, which is a surface-sensitive technique due to the amount residing in the samples' bulk side.

3.2. Verification of Electrochemical and Optical Tunability of the TiO_2 Layers. The electrochemical properties during lithiation and delithiation were studied in a half-cell configuration to generate insights into the mechanism behind optical tunability. The overall redox reaction during coloration (lithiation) and bleaching (delithiation) is shown in eq 5. Four ECDs are constructed containing TiO_2 nanofibrous layers (Figure 1) with and without NPs (Ag, Au, and CuO). During the cathodic potential (Figure 2a), the synchronous injection of positive ions and electrons into the nanofibers leads the layer to switch to the colored state.[41] This process is shown in Figure 2a between −1.7 and − 2 V and represents a phase transition from a TiO_2 to Li_xTiO_2. Conversely, during the anodic potential scan, a broad peak with j_{max} between −0.35 and −0.65 V is found and associated with the ejection of counterions and electrons, inducing the bleaching of the nanofibrous film, making its appearance transparent.[45] For the overall redox reaction, it is known that structural phase changes might occur mainly during the lithiation of TiO_2 nanostructures.[46,47] Depending on the TiO_2 phase, the coloration reversibility can deeply be affected without a guarantee for complete delithiation. An example of this case is the structural change known during lithiation from rutile (delithiated) to an intermediate monoclinic (fully lithiated) phase.[46]

$$x\mathrm{Li}^+ + \mathrm{TiO_2} + x\mathrm{e}^- \rightleftarrows \mathrm{Li}_x\mathrm{TiO_2} \quad (5)$$

From the results in Figure 2a, the profound effect of NPs in the cathodically color changing TiO_2 nanofibers is clear. The region of interest is from the −2 to 0 V region as the electrochromically active material here is TiO_2 and the Li^+ source electrolyte is nonaqueous. The obtained results are in good agreement with the charge evolution measurements in Figure 2b. Among the samples, the Au/TiO_2 composite showed the most prominent electrochemical activity with an anodic current density of 1.81 mA/cm^2 and an areal capacitance of 312 F/cm^2 in the EC layer form. The CuO/TiO_2 with a 1.33 mA/cm^2 anodic peak and 217 F/cm^2 in areal

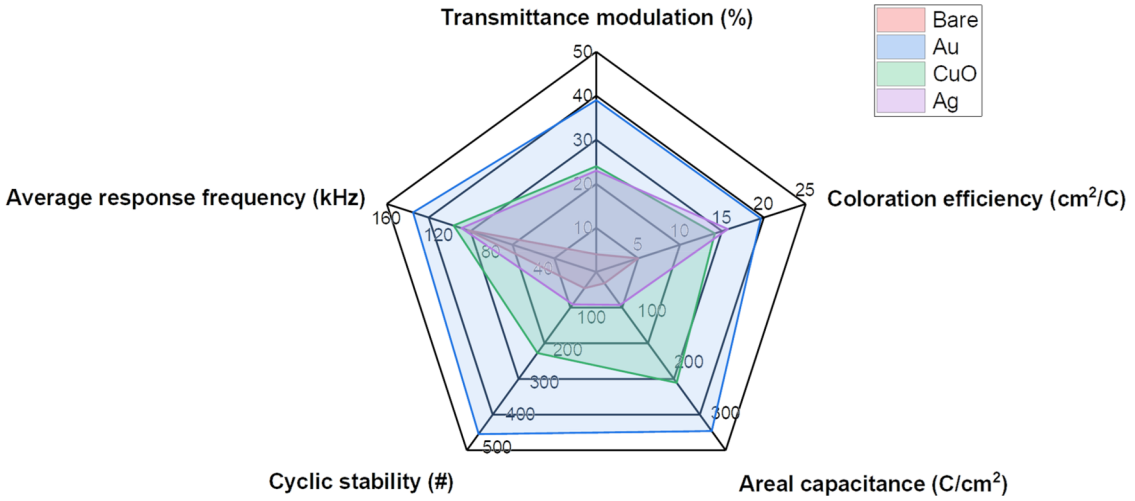

Figure 6. Radar plot showing the dominance of different ECDs over each other for average color modulation time, transmittance modulation, coloration efficiency, areal capacitance, and cyclic stability. Note that the first 500 stability cycles conducted as a requirement of the general fabrication protocol and 1000 cycles are measured in total for the Au/TiO_2 sample.

https://doi.org/10.1021/acsanm.1c02231
ACS Appl. Nano Mater. 2021, 4, 8600−8610

capacitance is second best. For Ag/TiO_2, a 0.39 mA/cm^2 anodic peak and 64 F/cm^2 areal capacitance are found, while for the bare TiO_2, lower values are obtained, i.e., a 0.19 mA/cm^2 anodic peak with 22 F/cm^2 areal capacitance. These results can be correlated to the increased conductivity, and hence increased electrochemical activity, of modified nanofibers due to the effect of NP doping.[48−50] EIS spectra of the measured samples yielded results in parallel to this case, such that the charge transfer resistance (Rct) values are 18.75 Ω for bare TiO_2, 11.84 Ω for Ag/TiO_2, 10.46 Ω for Au/TiO_2, and 19.17 Ω for CuO/TiO_2. Corresponding Nyquist plots of the EIS scans are given in Figure S8.

The optical changes for ECDs were estimated by combining UV−vis spectroscopy and chronoamperometry (CA). In a typical CA experiment, each cycle is measured during charging (coloration) for 30 s, followed by discharge (bleaching) throughout 30 s (e.g., Au/TiO_2, Figure 2b). Before bleaching, the transmittance spectrum was recorded at the 10, 20, 30, 40, and 50 cycles. The transmittance (% T) spectra for the colored (solid line) and bleached (dashed line) states are presented in Figure 3a. The corresponding optical density modulation of each ECD throughout 3250 s is shown in Figure 3b. It is clearly seen from these results that the most effective optical density change is obtained for Au/TiO_2 composite fibers, which exhibit a stable ΔT ($T_b - T_c$ @700 nm) = 40%. CuO/TiO_2 ECD has a similar trend as the ECD with Au/TiO_2 with ΔT = 23% averaged over 50 cycles. Ag-composited fibers show decay in optical modulation from the 30th cycle onward. At the 50th cycle, only half of the initial optical density change remains, which corresponds to ΔT = 12%. In this study, the bare TiO_2 fibers are shown to be deficient in terms of their optical response with an averaged ΔT of 4%. The results suggest that compositing TiO_2 fibers with NPs can have a tremendous effect in terms of electrochromic response so that compositing NPs can provide a more efficient lithiation during the coloration process.

Different metal and metal oxide NPs used in this study proved to enhance the electrochromic response of TiO_2 fibers. The results obtained by using Ag and CuO NPs do not meet with the one observed for the Au NP composited. This can be explained by irreversible lithiation since coloration and bleaching occur via a redox reaction (eq 5) in the EC layer. If the delithiation process cannot take place, e.g., highly stable lithiated redox products are formed, it might no longer be possible to convert ECDs back into the transparent state, and no further lithiation can take place upon changing the polarity of the applied potential difference. Therefore, poor cyclic performance observed in Ag-composited and bare TiO_2 fibers can be linked to the rapid decay of the electrochromic layer in the device forms caused by entrapped Li^+ ions, similar to what was observed in Li-ion batteries.[51] In Figure S9a, an example of complete delithiation is presented for a TiO_2 EC layer, where lithiation does not take place after the 6th cycle, proving the point of decaying performance. No difference in transmittance between the two states was observed once the reversible lithiation/delithiation behavior was lost.

3.3. Band Gap Modulation Via Metal/Metal Oxide Nanoparticles. To derive a mechanism and design rules for color tunability in this novel type of nanofiber architectures modified with NPs, the optical properties are examined in detail. Pristine NPs loaded on TiO_2 nanofibers were deposited over FTO/glass substrates to form the EC layer. After fabrication, the samples were analyzed with a UV−vis spectrometer. A comparison of the UV−vis spectra for Ag, Au, and CuO supported on TiO_2/FTO/glass is displayed in Figure 4a. As the first effect observed for the nanofibers loaded with NPs, a 10% decrease in transmittance at 700 nm is found when compared to the bare TiO_2 nanofiber layer. It is possible to experimentally verify the light absorptance for each nanofiber design containing metal (Ag and Au) and metal oxide (CuO) nanofibers provided in Figure 4a. In the spectra, it is clearly reflected that each of the FTO substrates with TiO_2 nanofibers loaded with NPs can yield an increase in absorptance at a wavelength (λ) = 310 nm. As for λ > 310 nm, absorptance decreases and remains about 20% (absorptance y-axis), with the bare TiO_2 as the lowest in absorption at 10% (absorptance y-axis). This observation can be rationalized because our source of excitation is light, and therefore, it is necessary to explain the light-absorptance effects from Figure 4a. The light-absorptance for the TiO_2 nanofibers can primarily be ascribed to rutile presence with a distinctive absorption between 300−400 nm. The increase in absorptance and the small blue-shift in the absorption spectra for the TiO_2 nanofibers loaded with NPs is attributed to the charge-carrier separation.[52,53] This mechanism could also contribute to the overall charge transfer and coloration, like the depletion of the band gap energy levels.[54] No clear absorption peak from the embedded Au or Ag NPs is observed in Figure 4a, which also indicates that no plasmonic activity is detected. This is owing to the low amount of NPs embedded in the TiO_2 nanofibers.

To discriminate between the effects, the impact of NPs in the TiO_2 semiconductor are investigated by estimating the band gap in Figure 4b. Depending on the NPs/TiO_2 composition, the band gap can be blue-shifted, e.g. for TiO_2, Ag/TiO_2, Au/TiO_2, and CuO/TiO_2 is 2.90 eV, 2.85 eV, 2.80 eV, and 2.72 eV. In general, the band gap results are well aligned with Figure 4a and suggest that the addition of NPs reduces the formation of energy levels in the forbidden energy gap of TiO_2,[55,56] while maintaining charge carrier's separation. It is also possible to link the results of the optical measurements with the charge storage experiments given in Figure 2b. For Au NPs, the charge storage reaches the highest when compared to the other NPs. This can be explained by the formation of a reversible Au−Li alloy phase during lithiation−delithiation cycles extending the lifetime of the EC layer, as revealed in Figure S10a,b.[57] Here, 1000 cycles are measured; the first 500 cycles, which takes 8 h to complete, are conducted as a requirement of the general characterization protocol of this study; however, since the ECD showed exceptional functional performance, 500 cycles were additionally carried out for prolonged usage probation. For other NPs like Ag, Li could have a more profound effect by either poisoning or reducing the reversible conversion of the metal by creating a more stable Ag−Li phase during lithiation. For oxides, like Cu_2O or Ag_2O suggested by XPS in Figure 1, the lithiation goes via the oxidation of Li and subsequent reduction of the NP to a metal state. This is followed by the formation of the metal (M)−Li phase with reduced reversibility as clearly observed in Figure S11 for EC layers loaded with Ag and CuO NPs.[58,59] In these tests, the ECDs were subjected to 500 cycles, whereas the EC layers loaded with Ag NPs lasted for 50 cycles, and CuO NPs lasted for 200 cycles. Note that bare TiO_2 EC layers could not survive for more than 50 cycles, and hence the results are not shown.

Besides the reversibility during lithiation and delithiation, ECD performance is attributed to the chemical stability and

https://doi.org/10.1021/acsanm.1c02231
ACS Appl. Nano Mater. 2021, 4, 8600−8610

redox potential of each NP employed. Electron transfer from the semiconductor vacancies to the interface of metal NPs (e.g., Au), as seen in XPS, may also be able to boost charge separation, allowing coloration tunability and high coloration efficiency.[60,61] Metal NPs in contact with the TiO_2 fibers lead to a spatial change in the band structures. A band bending occurs depending on the nature of the contact, such that, for the case of Au, a higher work function of the Au NPs will lead to a Schottky contact, while for Ag NPs, it will result in an Ohmic contact.[62] Expected band structures for Ag- and Au-decorated TiO_2 nanofibers are provided in Scheme S1 in the Supporting Information together with the ultraviolet photoelectron spectroscopy (UPS) scans provided in Figure S12. Altered band structures here can be the main reason for the difference in the energy band gap values of pristine and NP-containing TiO_2. Evident changes in the energy levels are summarized in Table S1 by comparing EC layers of bare TiO_2 with NP composited ones.

Additionally, the presence of the oxidized form of Ag (e.g., Ag_2O) or already oxidized CuO phases could enable heterojunction formation with TiO_2 (i.e., band alignment).[63] This mechanism is significantly different when compared to not deeply oxidized metal NPs (e.g., Au). Band alignment[62] between CuO and TiO_2 may be expected and help to improve the coloration response of the TiO_2 nanofibers in terms of transmittance difference between colored and bleached states. The latest can be judged on the basis of the electron affinity and the Fermi level position between CuO and TiO_2, which can easily stimulate electron and hole recombination.[64,65] Results of the aforementioned effects causing differences on the band structure by interfacing metal (oxide) NPs and TiO_2 are verified by the UV−vis−NIR measurements and given in Figure 4b, with the highest band gap shift found around 2.72 eV. Such variations on the band gap values can also contribute to color change in EC layers.

3.4. Design Rules for Color Modulation in Electrochromic Devices Containing TiO_2 Nanofibers Loaded with Nanoparticles. One of the most critical operating parameters in ECDs is coloration efficiency (CE), which is closely related to the energy supply processes, i.e., application of an electrical potential upon coloration. The CE of different ECDs is plotted against time in Figure S13. It can be observed in Table 2 that the highest coloration efficiencies are achieved for the Au/TiO_2 ECD with a CE of 24 cm^2/C. This is the result of Au NPs facilitating an easier lithiation/delithiation for TiO_2 nanofibers by increasing the conductivity, which is already reflected by the smaller voltage difference between anodic and cathodic peaks in CV for Au-composited fibers in Figure 2. However, the lack of contact and the energy barrier caused by the contact potential between NPs and nanofibers still creates an extra energy barrier to achieve a further increase in coloration efficiency values.[66,67] The decay observed in optical density change in Ag-composited fibers still persists, as reflected in Figure 3b, which means that even the areal capacitance cannot compensate for the optical modulation for the Ag-based ECD structure. The TiO_2/CuO ECD, on the other hand, has a similar trend as the Au-composited TiO_2 fibers. Here, coloration efficiency seems to be stable over 50 cycles and stays around 14.86 cm^2/C. Lastly, bare TiO_2 fibers show the least efficiency for coloration. The decay in performance is also reflected in the coloration efficiency, which means that bare nanofibers cannot be used as EC layers.

Another key parameter for ECD is coloration and bleaching time. Fast response times are associated with a porous active electrode, which enables rapid lithiation/delithiation. It is known that coloration time is a function of active surface area, i.e., area exposed to the electrolyte, which can be tailored by using different fabrication techniques, listed in Table S2. Among them, the increased surface area is limited in a 2D configuration, while electrospinning allows 3D nanofiber formulations. Therefore, taking advantage of the third dimension, it is possible to decrease the response time of the device by modifying the active surface area of the EC layers. This study shows that the use of composited nanofibers can attain modulation times by 6 s without losing performance in terms of optical density modulation with a total of 1000 cycles without altering performance (Figure S10). Typically, the average coloration times span between 180 and 2 s at a limited number of cycles (Table S2) over a restricted active area. Our results demonstrate that for large area EC layers and in situ additive NP loading, co-axial electrospinning is an excellent option.

Results from Table S2 revealed that the fabrication method plays an important role in the device performance, resulting from the final layer structure quality obtained. Thin film is the most widely used type of TiO_2 EC layers, which results in variable color modulation time and poor cyclic performance. This can be linked to the stress induced by cyclic lithiation/delithiation processes. Continuous expansion and contraction of the active surface area can cause inelastic mechanical deformation and material loss from the surface, leading to performance decay over time.[68,69] 1D structures such as wires, rods, and tubes can be a remedy to overcome cyclic stress-induced cracking with cyclic lifetimes up to 1000 cycles.[70] In this study, it is shown that the same performance can be achieved with ECD-based Au/TiO_2 nanofibers, i.e., continuous usage over 18 h with cycling, with faster coloration time. With electrospinning, it is possible to obtain high-quality EC layers with an option to incorporate decorative/compositing NPs over large extended areas. NPs are useful not only for prolonging the cycle life but also for engineering the band structure so that the obtained color in the ECD can be tailored. Our results suggest that the ECD formed with NP-composited TiO_2 fibers can yield different colors such that bare TiO_2 gives a pale blue color; while Ag/TiO_2, Au/TiO_2, and CuO/TiO_2 yield brown, dark blue, and dark green colors, respectively. A representative image of the colored ECDs is given in Figure 5.

Each ECD constructed device is shown in Figure 6, including optoelectronic parameters important for ECD assembly. Among the fabricated ECD, Au/TiO_2 is the option of choice because of its excellent transmittance modulation, coloration efficiency, areal capacitance, cyclic stability, and averaged modulation time. This is the first time to our knowledge that composited electrospun fibers are used to tune the modulated color of the assembled ED layers in the ECDs.

4. CONCLUSIONS

EC layers with composite nanofibers as the active layer were fabricated by using co-axial electrospinning. This method enables the fabrication of EC layers allowing color modulation via in situ NP decoration during electrospinning. STEM, EDX, and XPS results proved that compositing NPs are present both on the fiber surface and embedded inside. TiO_2 fibers composited with Ag, Au, and CuO NPs were tested and were shown to have distinct optoelectronic properties. A blue

https://doi.org/10.1021/acsanm.1c02231
ACS Appl. Nano Mater. 2021, 4, 8600−8610

shift in the optical band gap was observed in composited nanofibers such that E_g values for the TiO_2, Ag/TiO_2, Au/TiO_2, and CuO/TiO_2 are 2.9, 2.85, 2.8, and 2.72 eV, respectively. ECDs assembled with the aforementioned layers were tested electrochemically until failure, and it was shown that 1000 cycles can be achieved with Au/TiO_2 type of EC layers. Detailed analysis of CA measurements coupled with UV−vis−NIR spectroscopy for the same device showed that a color modulation time of 6 s with a transmittance modulation of 40% can be obtained, which translates into a coloration efficiency of 20 cm^2/C. Based on the very promising device performance provided by Au/TiO_2 nanofibers, it is possible to foresee that large scale fabrication by electrospinning of EC layers can become an interesting future route to the new generation of smart colored windows.

■ ASSOCIATED CONTENT

Supporting Information

The Supporting Information is available free of charge at https://pubs.acs.org/doi/10.1021/acsanm.1c02231.

Band structure changes in TiO_2 upon contact with Au and Ag NPs, transmittance and reflectance spectra recorded for FTO coated substrates, SEM images of non-annealed and annealed NP-composited TiO_2 fibers, STEM images of the NP-composited TiO_2 fibers, SAED of the TiO_2 nanofibers, XRD pattern of bare and NP-composited TiO_2 fibers, EDX spectra and EDX map of the Au signal obtained from nanofibers composited with Au NPs, bright field-TEM images of the NPs, Nyquist plots obtained from potentiodynamic EIS before cycling, CA scans performed on bare and NP-composited TiO_2 fibers, UPS spectra of bare and NP-composited TiO_2 fibers, energy levels and work functions of bare and NP-composited TiO_2 fibers, CE values of bare and NP-composited TiO_2 fibers over time, comparison of coloration and bleaching times for TiO_2-based ECD layers (PDF)

■ AUTHOR INFORMATION

Corresponding Authors

Cavit Eyovge − *Mesoscale Chemical Systems, MESA+ Institute, University of Twente, 7522 NB Enschede, the Netherlands;* orcid.org/0000-0002-2805-0742; Email: c.eyovge@utwente.nl

Arturo Susarrey-Arce − *Mesoscale Chemical Systems, MESA+ Institute, University of Twente, 7522 NB Enschede, the Netherlands;* orcid.org/0000-0003-2572-223X; Email: a.susarreyarce@utwente.nl

Han Gardeniers − *Mesoscale Chemical Systems, MESA+ Institute, University of Twente, 7522 NB Enschede, the Netherlands;* orcid.org/0000-0003-0581-2668; Email: j.g.e.gardeniers@utwente.nl

Authors

Cristian S. Deenen − *Mesoscale Chemical Systems, MESA+ Institute, University of Twente, 7522 NB Enschede, the Netherlands*

Francisco Ruiz-Zepeda − *Department of Materials Chemistry, National Institute of Chemistry, 1000 Ljubljana, Slovenia*

Stephan Bartling − *Leibniz Institute for Catalysis, D-18059 Rostock, Germany;* orcid.org/0000-0001-5901-7235

Yury Smirnov − *Inorganic Materials Science, MESA+ Institute, University of Twente, 7522 NB Enschede, the Netherlands*

Monica Morales-Masis − *Inorganic Materials Science, MESA + Institute, University of Twente, 7522 NB Enschede, the Netherlands;* orcid.org/0000-0003-0390-6839

Complete contact information is available at: https://pubs.acs.org/10.1021/acsanm.1c02231

Author Contributions

All authors have given approval to the final version of the manuscript.

Funding

C.E., C.S.D., A.S.-A., and H.G. received funding from the European Research Council (ERC) under the European Union's Horizon 2020 research and innovation program (grant agreement no. 742004). F.R.-Z. received funding from the Slovenian Research Agency (programs P2-0393 and P2-0132).

Notes

The authors declare no competing financial interest.

■ ACKNOWLEDGMENTS

The authors would also like to thank Mark Smithers for performing HRSEM imaging. The authors acknowledge fruitful discussions from Goran Dražić.

■ REFERENCES

(1) Granqvist, C. G. Electrochromics for smart windows: Oxide-based thin films and devices. *Thin Solid Films* **2014**, *564*, 1−38.

(2) Mortimer, R. J.; Dyer, A. L.; Reynolds, J. R. Electrochromic Organic and Polymeric Materials for Display Applications. *Displays.* **2006**, *27*, 2−18.

(3) Lahav, M.; van der Boom, M. E. Polypyridyl Metallo-Organic Assemblies for Electrochromic Applications. *Adv. Mater.* **2018**, *30*, 1706641.

(4) Eren, E.; Karaca, G. Y.; Koc, U.; Oksuz, L.; Oksuz, A. U. Electrochromic characteristics of radio frequency plasma sputtered WO3 thin films onto flexible polyethylene terephthalate substrates. *Thin Solid Films* **2017**, *634*, 40−50.

(5) Pan, L.; Han, Q.; Dong, Z.; Wan, M.; Zhu, H.; Li, Y.; Mai, Y. Reactively sputtered WO3 thin films for the application in all thin film electrochromic devices. *Electrochim. Acta* **2019**, *328*, 135107.

(6) Chang, J. Y.; Chen, Y. C.; Wang, C. M.; Wang, W. N.; Wen, C. Y.; Lin, J. M. Electrochromic Properties of Lithium-Doped Tungsten Oxide Prepared by Electron Beam Evaporation. *Coatings* **2019**, *9*, 191.

(7) Dinh, N. N.; Oanh, N. T. T.; Long, P. D.; Bernard, M. C.; Goff, A. H. L. Electrochromic properties of TiO2 anatase thin films prepared by a dipping sol-gel method. *Thin Solid Films* **2003**, *423*, 70−76.

(8) Ye, T.; Xiang, Y.; Ji, H.; Hu, C.; Wu, G. Electrodeposition-Based Electrochromic Devices with Reversible Three-State Optical Transformation by Using Titanium Dioxide Nanoparticle Modified FTO Electrode. *RSC Adv.* **2016**, *6*, 30769−30775.

(9) Liu, S.; Qu, X. Construction of Nanocomposite Film of Dawson-Type Polyoxometalate and TiO2 Nanowires for Electrochromic Applications. *Appl. Surf. Sci.* **2017**, *412*, 189−195.

(10) Wei, D.; Scherer, M. R. J.; Bower, C.; Andrew, P.; Ryhanen, T.; Steiner, U. A Nanostructured Electrochromic Supercapacitor. *Nano Lett.* **2012**, *12*, 1857−1862.

(11) Chen, J. Z.; Ko, W. Y.; Yen, Y. C.; Chen, P. H.; Lin, K. J. Hydrothermally Processed TiO2 Nanowire Electrodes with Antireflective and Electrochromic Properties. *ACS Nano* **2012**, *6*, 6633−6639.

(12) Reyes-Gil, K. R.; Stephens, Z. D.; Stavila, V.; Robinson, D. B. Composite WO3/TiO2 Nanostructures for High Electrochromic Activity. *ACS Appl. Mater. Inter.* **2015**, *7*, 2202−2213.
(13) Mjejri, I.; Gaudon, M.; Rougier, A. Mo addition for improved electrochromic properties of V2O5 thick films. *Sol Energy Mater Sol C* **2019**, *198*, 19−25.
(14) Kim, K. H.; Koo, B. R.; Ahn, H. J. Effects of Sb-doped SnO2-WO3 nanocomposite on electrochromic performance. *Ceram. Int.* **2019**, *45*, 15990−15995.
(15) Park, K. W.; Song, Y. J.; Lee, J. M.; Han, S. B. Influence of Pt and Au nanophases on electrochromism of WO3 in nanostructure thin-film electrodes. *Electrochem. Commun.* **2007**, *9*, 2111−2115.
(16) Cai, G. F.; Wang, X. L.; Zhou, D.; Zhang, J. H.; Xiong, Q. Q.; Gu, C. D.; Tu, J. P. Hierarchical structure Ti-doped WO3 film with improved electrochromism in visible-infrared region. *RSC Adv.* **2013**, *3*, 6896−6905.
(17) Kahattha, C.; Noonuruk, R.; Pecharapa, W. Effect of Titanium Dopant on Physical and Optical Properties of Wo3 Thin Films Prepared by Sol-Gel Method. *Suranaree J. Sci. Tech.* **2019**, *26*, 37−43.
(18) He, T.; Ma, Y.; Cao, Y.; Yang, W.; Yao, J. Enhanced electrochromism of WO3 thin film by gold nanoparticles. *J. Electroanal. Chem.* **2001**, *514*, 129−132.
(19) He, T.; Ma, Y.; Cao, Y. A.; Yang, W. S.; Yao, J. N. Improved photochromism of WO3 thin films by addition of Au nanoparticles. *Phys. Chem. Chem. Phys.* **2002**, *4*, 1637−1639.
(20) Kharade, R. R.; Mali, S. S.; Patil, S. P.; Patil, K. R.; Gang, M. G.; Patil, P. S.; Kim, J. H.; Bhosale, P. N. Enhanced electrochromic coloration in Ag nanoparticle decorated WO3 thin films. *Electrochim. Acta* **2013**, *102*, 358−368.
(21) Hoseinzadeh, S.; Ghasemiasl, R.; Bahari, A.; Ramezani, A. H. The injection of Ag nanoparticles on surface of WO3 thin film: enhanced electrochromic coloration efficiency and switching response. *J. Mater. Sci-Mater El* **2017**, *28*, 14855−14863.
(22) Sakar, M.; Mithun Prakash, R.; Trong-On, D. Insights into the TiO2-based photocatalytic systems and their mechanisms. *Catalysts* **2019**, *9*, 680.
(23) Tebyetekerwa, M.; Ramakrishna, S. What Is Next for Electrospinning? *Matter* **2020**, *2*, 279−283.
(24) Cavaliere, S.; Subianto, S.; Savych, I.; Jones, D. J.; Roziere, J. Electrospinning: designed architectures for energy conversion and storage devices. *Energy Environ. Sci.* **2011**, *4*, 4761−4785.
(25) Santangelo, S. Electrospun Nanomaterials for Energy Applications: Recent Advances. *Appl. Sci.* **2019**, *9*, 1049.
(26) Adhikari, S.; Sarkar, D. Synthesis and Electrochemical Properties of Nanocuboid and Nanofiber WO3. *J. Electrochem. Soc.* **2015**, *162*, H58−H64.
(27) Dulgerbaki, C.; Maslakci, N. N.; Komur, A. I.; Oksuz, A. U. Electrochromic strategy for tungsten oxide/polypyrrole hybrid nanofiber materials. *Eur. Polym. J.* **2018**, *107*, 173−180.
(28) Chang, W.; Xu, F.; Mu, X.; Ji, L.; Ma, G.; Nie, J. Fabrication of nanostructured hollow TiO2 nanofibers with enhanced photocatalytic activity by coaxial electrospinning. *Mater. Res. Bull.* **2013**, *48*, 2661−2668.
(29) Liu, X.; Hu, Y. Y.; Chen, R. Y.; Chen, Z.; Han, H. C. Coaxial Nanofibers of ZnO-TiO2 Heterojunction With High Photocatalytic Activity by Electrospinning Technique. *Synth React Inorg M* **2014**, *44*, 449−453.
(30) Loscertales, I. G.; Barrero, A.; Guerrero, I.; Cortijo, R.; Marquez, M.; Gañán-Calvo, A. M. Micro/Nano Encapsulation via Electrified Coaxial Liquid Jets. *Science* **2002**, *295*, 1695−1698.
(31) Scofield, J. H. Hartree-Slater Subshell Photoionization Cross-Sections at 1254 and 1487ev. *J. Electron. Spectrosc.* **1976**, *8*, 129−137.
(32) Tauc, J.; Grigorovici, R.; Vancu, A. Optical Properties and Electronic Structure of Amorphous Germanium. *Phys. Status Solidi* **1966**, *15*, 627.
(33) Tauc, J.; Menth, A. States in the gap. *J. Non-Cryst. Solids* **1972**, *8-10*, 569−585.
(34) Whiticar, A. M.; Martensson, E. K.; Nygard, J.; Dick, K. A.; Bolinsson, J. Annealing of Au, Ag and Au-Ag alloy nanoparticle arrays on GaAs (100) and (111)B. *Nanotechnology* **2017**, *28*, 205702.
(35) Elishav, O.; Beilin, V.; Rozent, O.; Shter, G. E.; Grader, G. S. Thermal shrinkage of electrospun PVP nanofibers. *J. Polym. Sci., Part B: Polym. Phys.* **2018**, *56*, 248−254.
(36) Zhang, Z.; Zhang, L.; Hedhili, M. N.; Zhang, H.; Wang, P. Plasmonic Gold Nanocrystals Coupled with Photonic Crystal Seamlessly on TiO2 Nanotube Photoelectrodes for Efficient Visible Light Photoelectrochemical Water Splitting. *Nano Lett.* **2013**, *13*, 14−20.
(37) Zhang, D.; Wang, B.; Wang, J.; Wang, H.; Zhang, S.; Gu, D. Isolated/interacting Au islands on TiO2 NTs for the switching photocatalytic/photoelectrocatalytic degradation of refractory organic pollutants in wastewater. *RSC Adv.* **2019**, *9*, 2784−2791.
(38) Kaspar, T. C.; Droubay, T.; Chambers, S. A.; Bagus, P. S. Spectroscopic Evidence for Ag(III) in Highly Oxidized Silver Films by X-ray Photoelectron Spectroscopy. *J. Phys. Chem. C* **2010**, *114*, 21562−21571.
(39) Mosquera, A. A.; Albella, J. M.; Navarro, V.; Bhattacharyya, D.; Endrino, J. L. Effect of silver on the phase transition and wettability of titanium oxide films. *Sci. Rep.* **2016**, *6*, 32171.
(40) Hoflund, G. B.; Hazos, Z. F.; Salaita, G. N. Surface characterization study of Ag, AgO, and Ag2O using X-ray photoelectron spectroscopy and electron energy-loss spectroscopy. *Phys. Rev. B* **2000**, *62*, 11126−11133.
(41) Masoud, N.; Partsch, T.; de Jong, K. P.; de Jongh, P. E. Thermal stability of oxide-supported gold nanoparticles. *Gold Bull.* **2019**, *52*, 105−114.
(42) De Anda Villa, M.; Gaudin, J.; Amans, D.; Boudjada, F.; Bozek, J.; Evaristo Grisenti, R.; Lamour, E.; Laurens, G.; Macé, S.; Nicolas, C.; Papagiannouli, I.; Patanen, M.; Prigent, C.; Robert, E.; Steydli, S.; Trassinelli, M.; Vernhet, D.; Lévy, A. Assessing the Surface Oxidation State of Free-Standing Gold Nanoparticles Produced by Laser Ablation. *Langmuir* **2019**, *35*, 11859−11871.
(43) Fuggle, J. C.; Martensson, N. Core-Level Binding-Energies in Metals. *J. Electron. Spectrosc.* **1980**, *21*, 275−281.
(44) Li, J. Q.; Mei, Z. X.; Liu, L. S.; Liang, H. L.; Azarov, A.; Kuznetsov, A.; Liu, Y. P.; Ji, A. L.; Meng, Q. B.; Du, X. L. Probing Defects in Nitrogen-Doped Cu2O. *Sci. Rep.* **2014**, *4*, 7240.
(45) Meher, S. R.; Balakrishnan, L. Sol-gel derived nanocrystalline TiO2 thin films: A promising candidate for self-cleaning smart window applications. *Mater. Sci. Semicond. Process.* **2014**, *26*, 251−258.
(46) Kim, S. J.; Noh, S. Y.; Kargar, A.; Wang, D.; Graham, G. W.; Pan, X. In situ TEM observation of the structural transformation of rutile TiO2 nanowire during electrochemical, lithiation. *Chem. Commun.* **2014**, *50*, 9932−9935.
(47) Auer, A.; Steiner, D.; Portenkirchner, E.; Kunze-Liebhauser, J. Nonequilibrium Phase Transitions in Amorphous and Anatase TiO2 Nanotubes. *Acs Appl. Energ Mater.* **2018**, *1*, 1924−1929.
(48) Fang, D.; Huang, K.; Liu, S.; Li, Z. Electrochemical properties of ordered TiO2 nanotube loaded with Ag nanoparticles for lithium anode material. *J. Alloy Compd.* **2008**, *464*, L5−L9.
(49) Khan, M. M.; Ansari, S. A.; Lee, J.; Cho, M. H. Enhanced optical, visible light catalytic and electrochemical properties of Au@TiO2 nanocomposites. *J. Ind. Eng. Chem.* **2013**, *19*, 1845−1850.
(50) Zhang, W.; Liu, Y.; Li, W.; Liang, W.; Yang, F. Au nanocrystals decorated TiO2 nanotube arrays as anode material for lithium ion batteries. *Appl. Surf. Sci.* **2019**, *476*, 948−958.
(51) Manickam, M.; Singh, P.; Issa, T. B.; Thurgate, S. Electrochemical behavior of anatase TiO2 in aqueous lithium hydroxide electrolyte. *J. Appl. Electrochem.* **2006**, *36*, 599−602.
(52) Méndez-Medrano, M. G.; Kowalska, E.; Lehoux, A.; Herissan, A.; Ohtani, B.; Bahena, D.; Briois, V.; Colbeau-Justin, C.; Rodríguez-López, J. L.; Remita, H. Surface Modification of TiO2 with Ag Nanoparticles and CuO Nanoclusters for Application in Photocatalysis. *J. Phys. Chem. C* **2016**, *120*, 5143−5154.

https://doi.org/10.1021/acsanm.1c02231
ACS Appl. Nano Mater. 2021, 4, 8600−8610

(53) Grabowska, E.; Zaleska, A.; Sorgues, S.; Kunst, M.; Etcheberry, A.; Colbeau-Justin, C.; Remita, H. Modification of Titanium(IV) Dioxide with Small Silver Nanoparticles: Application in Photocatalysis. *J. Phys. Chem. C* **2013**, *117*, 1955−1962.
(54) Chen, F.; Huang, H.; Guo, L.; Zhang, Y.; Ma, T. The Role of Polarization in Photocatalysis. *Angew. Chem., Int. Ed.* **2019**, *58*, 10061−10073.
(55) Vasquez, G. C.; Taeno, M.; Maestre, D.; Cremades, A. Synthesis and Characterization of TiO2 Micro- and Nano-Structures with Variable Morphology and Aluminum Content. *Phys. Status Solidi A* **2018**, *215*, 1800249.
(56) Cremades, A.; Herrera, M.; Bartolome, J.; Vasquez, G. C.; Maestre, D.; Piqueras, J. On the thermal growth and properties of doped TiO2 and In2O3 elongated nanostructures and nanoplates. *Phys. B* **2014**, *453*, 92−99.
(57) Bach, P.; Stratmann, M.; Valencia-Jaime, I.; Romero, A. H.; Renner, F. U. Lithiation and Delithiation Mechanisms of Gold Thin Film Model Anodes for Lithium Ion Batteries: Electrochemical Characterization. *Electrochim. Acta* **2015**, *164*, 81−89.
(58) Paolella, A.; Brescia, R.; Prato, M.; Povia, M.; Marras, S.; De Trizio, L.; Falqui, A.; Manna, L.; George, C. Colloidal Synthesis of Cuprite (Cu2O) Octahedral Nanocrystals and Their Electrochemical Lithiation. *Acs Appl. Mater. Int.* **2013**, *5*, 2745−2751.
(59) Taillades, G.; Sarradin, J. Silver: high performance anode for thin film lithium ion batteries. *J. Power Sources* **2004**, *125*, 199−205.
(60) Naseri, N.; Azimirad, R.; Akhavan, O.; Moshfegh, A. Z. Improved electrochromical properties of sol-gel WO3 thin films by doping gold nanocrystals. *Thin Solid Films* **2010**, *518*, 2250−2257.
(61) Yu, Y.; Wen, W.; Qian, X. Y.; Liu, J. B.; Wu, J. M. UV and visible light photocatalytic activity of Au/TiO2 nanoforests with Anatase/Rutile phase junctions and controlled Au locations. *Sci. Rep.* **2017**, *7*, 41253.
(62) Kozlov, D. A.; Lebedev, V. A.; Polyakov, A. Y.; Khazova, K. M.; Garshev, A. V. The Microstructure Effect on the Au/TiO2 and Ag/TiO2 Nanocomposites Photocatalytic Activity. *Nanosyst. Physics, Chem. Math.* **2018**, *9*, 266−278.
(63) Liu, L.; Yang, W.; Sun, W.; Li, Q.; Shang, J. K. Creation of Cu2O@TiO2 Composite Photocatalysts with p-n Heterojunctions Formed on Exposed Cu2O Facets, Their Energy Band Alignment Study, and Their Enhanced Photocatalytic Activity under Illumination with Visible Light. *Acs Appl. Mater. Int.* **2015**, *7*, 1465−1476.
(64) Çinar, B.; Kerimoğlu, I.; Tönbül, B.; Demirbüken, A.; Dursun, S.; Cihan Kaya, I.; Kalem, V.; Akyildiz, H. Hydrothermal/electrospinning synthesis of CuO plate-like particles/TiO2 fibers heterostructures for high-efficiency photocatalytic degradation of organic dyes and phenolic pollutants. *Mater. Sci. Semicon. Proc.* **2020**, *109*, 104919.
(65) Kashiwaya, S.; Morasch, J.; Streibel, V.; Toupance, T.; Jaegermann, W.; Klein, A. The Work Function of TiO2. *Surfaces* **2018**, *1*, 73−89.
(66) Dhandayuthapani, T.; Sivakumar, R.; Ilangovan, R.; Gopalakrishnan, C.; Sanjeeviraja, C.; Sivanantharaja, A. High coloration efficiency, high reversibility and fast switching response of nebulized spray deposited anatase TiO2 thin films for electrochromic applications. *Electrochim. Acta* **2017**, *255*, 358−368.
(67) Rahmanzade, K. A.; Nikfarjam, A.; Ameri, M.; Mansoori, E. Improving Electrochromic Properties of WO3 Thin Film with Gold Nanoparticle Additive. *Int. J. Eng-Iran* **2015**, *28*, 1169−1174.
(68) Tang, X.; Chen, G.; Liao, H.; Li, Z.; Zhang, J.; Luo, J. Unveiling mechanical degradation for a monolithic electrochromic device: Glass/ITO/WO3/LiClO4 (PEO)/TiO2/ITO/glass. *Electrochim. Acta* **2020**, *329*, 135182.
(69) Wang, X.; Chen, K.; de Vasconcelos, L. S.; He, J.; Shin, Y. C.; Mei, J.; Zhao, K. Mechanical breathing in organic electrochromics. *Nat. Commun.* **2020**, *11*, 211.
(70) Qu, X.; Feng, H.; Liu, S.; Yang, Y.; Ma, C. Enhanced electrochromic performance of nanocomposite film based on Preyssler-type polyoxometalate and TiO2 nanowires. *Inorg. Chem. Commun.* **2018**, *98*, 174−179.

https://doi.org/10.1021/acsanm.1c02231
ACS Appl. Nano Mater. 2021, 4, 8600−8610